Soft Matter

Cite this: *Soft Matter*, 2012, **8**, 9870

www.rsc.org/softmatter

**PAPER**

# The influence of ionic strength on the adhesive bond stiffness of oral streptococci possessing different surface appendages as probed using AFM and QCM-D

**Adam L. J. Olsson,[a] Narasimhan Arun,[b] Johannes S. Kanger,[b] Henk J. Busscher,[a] Ivan E. Ivanov,[c] Terri A. Camesano,[c] Yun Chen,[a] Diethelm Johannsmann,[d] Henny C. van der Mei[a] and Prashant K. Sharma*[a]**

***Received 2nd May 2012, Accepted 17th July 2012***
**DOI: 10.1039/c2sm26025e**



Bacterial adhesion to surfaces poses threats to human-health, not always associated with adhering organisms, but often with their detachment causing contamination elsewhere. Bacterial adhesion mechanisms may not be valid for their detachment, known to proceed according to a visco-elastic mechanism. Here we aimed to investigate influences of ionic strength on the adhesive bond stiffness of two spherically shaped *Streptococcus salivarius* strains with different lengths of fibrillar surface appendages. The response of a Quartz-Crystal-Microbalance-with-Dissipation (QCM-D) upon streptococcal adhesion and changes in the ionic strength of the surrounding fluid indicated that the bond stiffness of *S. salivarius* HB7, possessing a dense layer of 91 nm long fibrils, was unaffected by ionic strength. Atomic-force-microscopic (AFM) imaging in PeakForce-QNM mode showed a small decrease in bond stiffness from 1200 to 880 kPa upon decreasing ionic strength from 57 to 5.7 mM, while Total-Internal-Reflection-Microscopy suggested a complete collapse of fibrils. *S. salivarius* HBV51, possessing a less dense layer of shorter (63 nm) fibrils, demonstrated a strong decrease in bond stiffness both from QCM-D and AFM upon decreasing the ionic strength, and a partial collapse of fibrils. Probably, the more hydrophobic and less negatively charged long fibrils on *S. salivarius* HB7 collapse side-on to the cell surface, while the more hydrophilic and negatively charged fibrils of *S. salivarius* HBV51 remain partially stretched. In summary, we demonstrate how a combination of different methods can yield a description of the structural changes occurring in the interfacial region between adhering, fibrillated streptococci and a substratum surface upon changing the ionic strength.

## Introduction

Microbial adhesion takes place on virtually all natural and man-made surfaces, as one of the initial steps in the formation of a biofilm.[1] Biofilms can pose considerable health threats in food processing, drinking water systems and human health. These threats are not always associated with adhering members of biofilm communities, but much more with detachment of biofilm organisms. In human health, for instance, contact lens related microbial keratitis is caused by transmission of bacteria adhering on lens cases to a contact lens onto the cornea, a process which requires both adhesion and detachment from the lens case and contact lens in order for the organisms to reach the cornea.[2] In food processing, detachment of thermo-resistant streptococci from heat exchanger plates in the downward, cooling section of pasteurizers can lead to contamination of already pasteurized milk.[3]

In order to influence initial microbial adhesion and detachment, understanding the adhesive bond at the bacterium–substratum interface is essential. According to the physico-chemical modelling, microbial adhesion is achieved by an interplay between attractive Lifshitz–van der Waals forces in combination with attractive or repulsive electrostatic and acid–base interactions.[4] Most physico-chemical models assume bacteria to be inert and rigid particles. In fact, bacteria possess a rigid inner-core, constituted by a layer of cross-linked peptidoglycan, that can be covered by various types of surface appendages and/or extracellular polymeric substances (EPS), which may affect their adhesion to surfaces. Due to this complexity, there are numerous examples in which physico-chemical models fail to explain bacterial adhesion to surfaces.[5] Since surface appendages or EPS often form the link between adhering bacteria and a

[a]*Department of Biomedical Engineering (FB40), W.J. Kolff Institute, University Medical Center Groningen and University of Groningen, P.O. Box 196, 9700 AD Groningen, The Netherlands. E-mail: p.k.sharma@umcg.nl; Fax: +31-50-363-3159; Tel: +31-50-3633140*
[b]*Nanobiophysics, MIRA Institute for Biomedical Technology and Technical Medicine, University of Twente, PO Box 217, 7500 AE, Enschede, The Netherlands*
[c]*Department of Chemical Engineering, Worcester Polytechnic Institute, Worcester, MA, USA*
[d]*Institute of Physical Chemistry, Clausthal University of Technology, D-38678 Clausthal-Zellerfeld, Germany*

substratum surface, appendages and EPS are likely to influence the mechanical properties of the bacterium–substratum bond. The bacterium–substratum bond has been described as visco-elastic and, as a consequence, microbial detachment requires extension of the adhesive bond by external forces before bond rupture occurs.[6] Oral biofilm left behind after toothbrushing, for instance, has appeared to be volumetrically expanded, which was attributed to the visco-elasticity of bonds between bacteria within the biofilm.[7] The visco-elastic properties of the adhesive bond between bacteria and surfaces are due to the presence of EPS and surface appendages attached to the cell membrane. Typically, bacteria may possess cell surface appendages of different lengths and widths like fibrils or fimbriae that may affect the adhesive bond, while EPS may be absent or present. Moreover, the conformation of these cell surface appendages and a possible EPS layer changes with time during initial adhesion[8] and is influenced by environmental factors, such as ionic strength and pH.[9]

Although microbial adhesion to surfaces has been amply studied in terms of the numbers of adhering bacteria and their time dependence, characterization of the adhesive bond stiffness between a bacterium and a substratum surface has remained experimentally challenging. Atomic Force Microscopy (AFM)[10] and optical tweezers[11] can both be applied to pull adhering bacteria away from a substratum surface after forced contact to yield the adhesion force. With the new PeakForce-QNM imaging mode in AFM, where force–distance curves obtained can be analyzed using Hertzian or DMT (Derjaguin–Muller–Toporov) theory, the stiffness of soft materials can be measured in terms of their Young's modulus.[12] However, such analyses have not been applied to estimate the stiffness of the adhesive bond of bacteria adhering on a substratum surface. Adhesive bond stiffness can also be assessed using a Quartz Crystal Microbalance (QCM-D). QCM-D senses adsorbed molecular films on an AT-cut quartz-crystal in terms of shifts in resonance frequency of the sensor-crystal and its dissipative energy losses.[13,14] The interpretation of the QCM-D response to bacterial adhesion on the quartz-crystal is less trivial than to molecular adsorption, as bacteria can be spherical or rod-shaped, fibrillated or fimbriated and are too large to couple to the sensor-crystal as a mass (*i.e.* conventional Sauerbrey-type mass-loading[15]) and bacterial adhesion to the QCM-D sensor-crystals surface has given rise to positive frequency shifts.[16–23] Rather, it has been demonstrated that bacteria adhering to the sensor-crystal in QCM-D form coupled resonators, with a resonance frequency of their own that is determined both by their mass and the stiffness of the adhesive bond.[24] The coupled resonance model was later applied to the adhesion of two spherical *Staphylococcus aureus* strains onto adsorbed fibronectin films to evaluate effects of staphylococcal fibronectin-binding-proteins on the adhesive bond stiffness.[24] The coupled resonance model has also been applied to rod-shaped *Pseudomonas aeruginosa* adhering to hydrophobic and hydrophilic substrata.[25] Therewith QCM-D is another technique through which adhesive bond stiffnesses can be obtained, but unlike AFM, in the absence of forced contact.

The aim of this study was to investigate the influence of ionic strength on the bond stiffness of two oral *S. salivarius* strains with different lengths of fibrils, using QCM-D and AFM. Possible stretching or collapse of fibrillar cell surface appendages on adhering bacteria upon changes in the ionic strength of the surrounding fluid was examined using Total Internal Reflection Microscopy (TIRM).

## Results

Plots of the shifts in frequency and bandwidth occurring upon bacterial adhesion to the QCM-D sensor-crystals surface and changes in ionic strength, normalized with respect to bacterial density $N_S$ (1/cm$^2$) at the sensor-surface ($\Delta f/N_S$ and $\Delta\Gamma/N_S$), display positive frequency shifts (see Fig. 1c and 2c for *S. salivarius* HB7 and HBV51, respectively). Due to the limited window of observable frequencies in the QCM-D, the frequency of zero-crossing[23] was not visible, but the data could be fitted to circles with different radii, confirming the validity of the coupled resonator model applied. The radius of the polar plots for *S. salivarius* HB7 is $6.8 \times 10^{-6}$ Hz per bacterium, regardless of ionic strength. On the other hand, the radii observed for *S. salivarius* HBV51 decreased from $3.3 \times 10^{-6}$ to $3.1 \times 10^{-6}$ down to $2.7 \times 10^{-6}$ Hz per bacterium upon decreasing the ionic strength from 57 to 12.5 and 5.7 mM, respectively.

The Young's moduli of the contact between a silicon nitride AFM tip and the two *S. salivarius* strains, derived using the PeakForce-QNM mode and DMT analysis, are presented in Fig. 1d and 2d for *S. salivarius* HB7 and HBV51, respectively. Importantly, adhesion forces between the tip and both streptococcal strains were less than 0.2 nN at all ionic strengths, confirming the validity of our choice to apply a Hertzian analysis, in which adhesion forces are neglected. The Young's modulus for *S. salivarius* HB7 decreased from 1.2 MPa to 0.88 MPa when the ionic strength decreased from 57 to 5.7 mM, with a change that was significant at $p < 0.05$ (Student's *t*-test). For *S. salivarius* HBV51, the corresponding decrease in Young's modulus occurred from 0.9 to 0.3 MPa, representing a highly significant difference ($p < 0.01$, Student's *t*-test).

TIRM was applied to determine changes in the bacterium–substratum separation distance upon decreasing the ionic strength of the surrounding fluid from 57 to 12.5 and 5.7 mM. Note that, as a limitation of TIRM, we could not report absolute values for the separation distance and actual separation distances for the bacteria at an initial ionic strength of 57 mM are unknown. The bacterium–substratum distances increase upon decreasing the ionic strength (Fig. 1e and 2e) and the largest increases in separation distance are observed upon reducing the ionic strength from 57 to 5.7 mM. For *S. salivarius* HB7, this increase amounted 88 nm, which corresponds to the known lengths of its fully extended long fibril (91 nm, as measured previously[26]). For *S. salivarius* HBV51, with its more sparsely distributed 63 nm long fibrillar surface appendages, bacteria were only displaced about 44 nm further away from the substratum surface upon reducing the ionic strength to 5.7 mM.

## Discussion

The stiffness of the adhesive bonds between adhering bacteria and a substratum surface plays an important role in detachment phenomena and is determined by the presence of EPS and appendages attached to the cell membrane. In this paper we evaluate the influence of the length and surface density of fibrillar

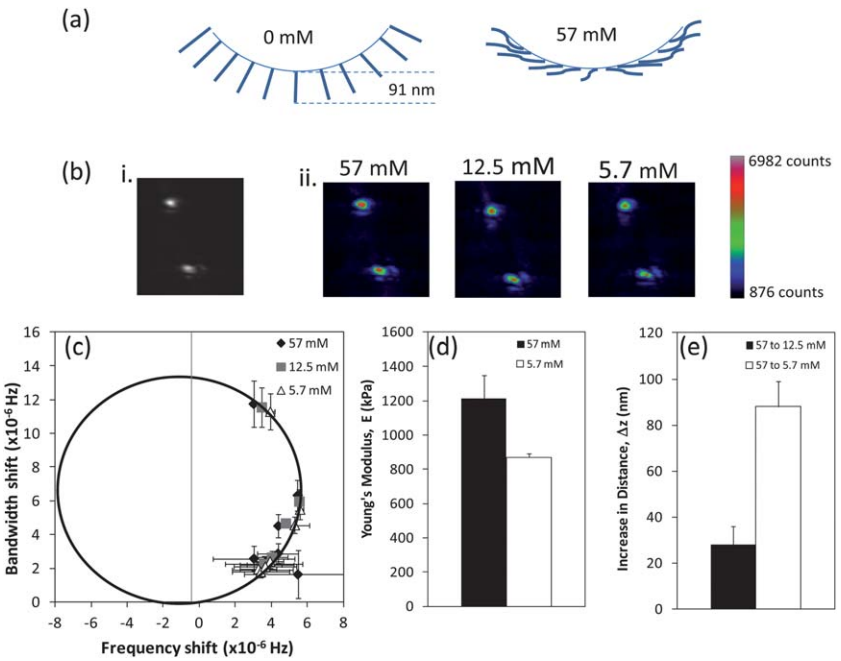


**Fig. 1** (a) Schematic presentation of the fibrillar surface appendages on *S. salivarius* HB7 in water (0 mM diagram, as obtained using electron microscopy after ruthenium red staining[24]) and their behaviour as a function of ionic strength, as concluded from the results of the current study. Upon increasing the ionic strength, the fibrils collapse and the fibrillar density close to the bacterial cell surface increases. (b) Example of a total internal reflection micrograph taken in black and white (i), and pseudo-colored for intensity at different ionic strengths (ii). (c) The shift in bandwidth as a function of shift in frequency per *S. salivarius* HB7 cell adhering to the QCM-D sensor surface. Circles indicate the best fit to the data, confirming the validity of the coupled resonance model for bacterial adhesion. The radii of the polar circles were $6.8 \times 10^{-6}$ Hz per bacterium, regardless of ionic strength. Error bars represent standard errors over three experiments with separately grown cultures. (d) Young's modulus of the bond between the *S. salivarius* cell surface and a silicon nitride, AFM tip. Error bars represent standard errors over at least 60 individual bacteria, divided over three experiments with separately grown cultures. (e) Increase in distance between adhering *S. salivarius* HB7 and a glass surface from its initial distance at 57 mM to lower ionic strengths of the suspending fluid (12.5 and 5.7 mM). Error bars represent standard errors over at least 6 individual bacteria, divided over three experiments with separately grown cultures.

surface appendages of two oral streptococcal strains on the adhesive bond stiffness at different ionic strengths. Using a coupled resonator model for analysis of the QCM-D response upon streptococcal adhesion and changes in ionic strength of the surrounding fluid, it was found that the bond stiffness of *S. salivarius* HB7, possessing a dense layer of 91 nm long fibrils as measured previously in water,[26] was not affected by ionic strength. AFM imaging in PeakForce-QNM mode showed a small decrease in bond stiffness from 1200 to 880 kPa upon decreasing the ionic strength from 57 to 5.7 mM, accompanied by a complete collapse of surface fibrils, as shown by TIRM (see schematics in Fig. 1a). *S. salivarius* HBV51, on the other hand, possessing a less dense layer of shorter (63 nm) fibrils,[26] demonstrated a clear decrease in bond stiffness both from QCM-D and AFM analyses upon a decrease in ionic strength, also accompanied by a collapse of fibrils but covering only two thirds of their lengths (see schematics in Fig. 2a).

Since an increase in ionic strength for adhering *S. salivarius* HB7 yields a decrease in separation distance between the bacterium and the substratum surface equal to the fibrillar length, this must indicate side-on collapse of the fibrils (see Fig. 1a). The shorter fibrils on *S. salivarius* HBV51 only yield a decrease in separation distance of two thirds of their length, which indicates that they remain partially stretched in the surrounding fluid (see Fig. 2a). This probably happens because the fibrils on *S. salivarius* HBV51 are more hydrophilic (27% removal by hexadecane from an aqueous suspension) and more negatively charged (zeta potential equals −22 mV) than the longer ones on *S. salivarius* HB7 (44% removal by hexadecane and a zeta potential of −18 mV).[27] Thus fibrils on *S. salivarius* HB7 will have a greater tendency to escape from the aqueous surrounding fluid and collapse on the cell surface than the more hydrophilic ones on *S. salivarius* HBV51, favouring an aqueous surrounding. In addition, since the fibrils on *S. salivarius* HBV51 are more negatively charged, they are also more strongly stabilized by electrostatic repulsion between fibrils. Note that our arguments only pertain to the behaviour of the surface fibrils on our spherical streptococci, and these may not be extrapolated to the behaviour of entire bacteria, as studied recently by QCM-D for fimbriated, rod-shaped Pseudomonas.[25]

Despite the differences in the working mechanism of AFM and QCM-D, the conclusions that can be drawn from both techniques support each other, although QCM-D failed to demonstrate any differences in adhesive bond stiffness at different ionic strengths for *S. salivarius* HB7. Note that in the case of *S. salivarius* HBV51, differences in adhesive bond stiffness were much larger at different ionic strengths and accordingly were revealed in the radii of the circular relationship between bandwidth and frequency shifts. Thus whereas on the one hand, both techniques support each other, it is puzzling why QCM-D fails to reveal a

 

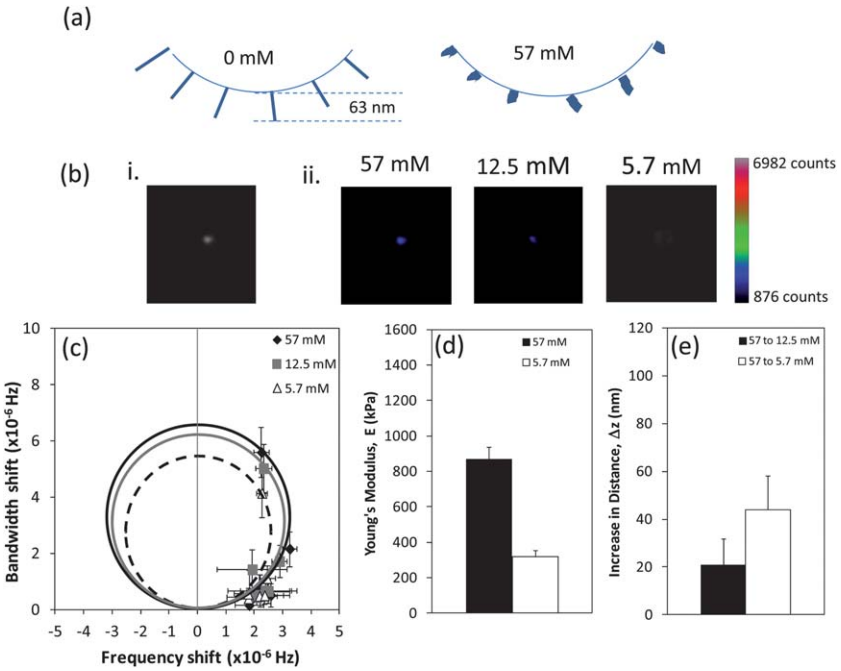


**Fig. 2** (a) Schematic presentation of the fibrillar surface appendages on *S. salivarius* HBV51 in water (0 mM diagram, as obtained using electron microscopy after ruthenium red staining[24]) and their behaviour as a function of ionic strength, as concluded from the results of the current study. Upon increasing the ionic strength, the fibrils collapse and the fibrillar density close to the bacterial cell surface increases. (b) See Fig. 1, now for *S. salivarius* HBV51. (c) See Fig. 1. Note that for *S. salivarius* HBV51 the radii of the circles decrease with increasing ionic strength from 3.3, 3.1 to $2.7 \times 10^{-6}$ Hz per bacterium for 57, 12.5 and 5.7 mM, respectively. (d) See Fig. 1, now for *S. salivarius* HBV51. (e) See Fig. 1, now for *S. salivarius* HBV51.

difference of about 300 kPa in bond stiffness for *S. salivarius* HB7. Both PeakForce-QNM AFM and QCM-D operate at relatively high frequencies of 1 kHz and 5 MHz, respectively, and this difference in operating frequency is unlikely to have such an influence. More likely, the time sequence in which changes in ionic strength were inferred to the system impacts the fibrillar collapse differently in QCM-D than in AFM. The AFM tip approaches the bacterial cell surface several minutes after changing the ionic strength while in QCM ionic strength is changed during measurements and adhesion to the sensor-crystal. Thus, whereas the AFM tip senses the fibrillar mass in a state that is fully adapted to its new ionic environment (*i.e.* either stretched or collapsed depending on ionic strength), stretching of already 'side-on' collapsed fibrils through a decrease in ionic strength in QCM-D first requires their detachment from the sensor-crystals surface.

In summary, this study demonstrates how a combination of different methods can yield a description of the structural changes occurring in the interfacial region between adhering, fibrillated streptococci and a substratum surface upon changing the ionic strength of the surrounding fluid. Moreover, it is indicated how these structural changes lead to differences in the adhesive bond stiffness between the streptococci and substratum surfaces.

## Experimental part

### Bacterial strains and growth conditions

*S. salivarius* mutant strains HB7 and HBV51 were cultured according to previously described protocols.[23] 10 mL pre-cultures were grown aerobically overnight at 37 °C in autoclaved Todd Hewitt broth (THB, Oxoid, Basingstoke, UK) and used to inoculate main-cultures of 200 mL of autoclaved THB. Main cultures were subsequently grown for 16 h at 37 °C to the early stationary phase. Bacteria were then harvested by centrifugation (5 min at 5000*g*) and washed in 100 mL adhesion buffer with an ionic strength of 57 mM (50 mM potassium chloride, 2 mM potassium phosphate and 1 mM calcium chloride, pH 6.8). Bacteria were sonicated intermittently 3 times for 10 s at 30 W (Vibra Cell model 375; Sonics and Materials, Danbury, CT) while cooling on ice, and once again washed in 100 mL buffer before being diluted in buffer to a final concentration of $3 \times 10^8$ bacteria per mL. Both strains are hydrophilic by their adhesion to hydrocarbons[27] and known not to produce any EPS, but they possess fibrillar surface appendages of different lengths and density, as schematically presented in Fig. 1a and 2a.[27] In demineralized water, *S. salivarius* HB7 possesses a dense layer of 91 nm long fibrils, whereas *S. salivarius* HBV51 has a sparse layer of 63 nm long fibrils.

### QCM-D and analysis

Bacterial adhesion was carried out in a window-equipped QCM-D device (model Q-sense E1, Q-sense, Gothenburg, Sweden) on gold-plated QCM-D sensor-surfaces. Before each experiment, the sensor-crystals' surfaces were cleaned by immersion in a 3 : 1 : 1 mixture of ultrapure water, $NH_3$ and $H_2O_2$ (Merck, Darmstadt, Germany) at 70 °C for 10 min followed by 10 min UV/Ozone treatment, yielding a water contact angle after UV/Ozone treatment at 16 ± 3 degrees. Cleaned sensor-crystals'

surfaces were immediately placed in the QCM-D and bacterial adhesion was allowed from the high ionic strength buffer (57 mM) for 1 h at 20 °C and at a flow rate of 300 μL $min^{-1}$. The QCM-D flow chamber is disc-shaped with a volume of approximately 100 μL and a diameter of 12 mm with inlet and outlet facing the crystal surface, giving an estimated shear rate of 2.8 $s^{-1}$. After adhesion, the bacterial suspension in 57 mM ionic strength buffer was replaced by 12.5 or 5.7 mM buffer, without suspended bacteria, at intervals of 5 min. Changes in $\Delta f$ and $\Delta\Gamma$ due to differences in ionic strength of the buffers were accounted for by subtracting the QCM-D responses $\Delta f$ and $\Delta\Gamma$ upon changing ionic strength in the absence of bacteria from the ones measured in a 57 mM buffer in the presence of bacteria.

Images of bacterial deposition on the QCM-D sensor-crystal were collected 30 s before each reduction in ionic strength, using a CCD camera (Model A101, Basler vision technologies, Ahrensburg, Germany), mounted on a metallurgical microscope with a 20× objective (Leica DM2500 M, Rijswijk, The Netherlands). The bacterial density, *i.e.* the number of bacteria adhering per unit area $N_S$ ($1/cm^2$), was calculated from these images using in-house image analysis software (written on the MATLAB platform). Analysis of these images did not reveal any significant difference in the number of bacteria adhering on the sensor-crystal surface upon changes in ionic strength (data not shown). All measurements were performed in triplicate with separately cultured bacteria.

The QCM-D data were analyzed using a coupled resonance model which has previously been described in terms of frequency shifts in air[29] and in terms of both frequency and bandwidth shifts in liquid.[24,28,30] In the coupled resonance model, particles or in the present case bacteria adhering to the sensor-crystal surface are depicted as resonators with their own resonance frequency ($f_b$) according to eqn (1) that couples to the resonance frequency of the QCM-D sensor-surface ($f_s$) according to eqn (2)

$$2\pi f_b = \sqrt{\frac{k^*}{m}} \tag{1}$$

$$\omega = 2\pi f_s = \sqrt{\frac{K}{M}} \tag{2}$$

where $K$ and $M$ are the stiffness and mass, respectively, of the QCM-D sensor-crystal, $m$ is the mass of the bacterium and $k^*$ is the complex stiffness of the bacterial-sensor bond, which can be written as

$$k^* = k + i\omega\xi \tag{3}$$

where $k$ is the stiffness of the spring and $\xi$ is the drag coefficient of the dashpot giving rise to the shift in bandwidth, $\Gamma$. Note that the bandwidth $\Gamma$ is related to the traditionally measured dissipation $D$ according to

$$\Delta\Gamma = \Delta Df/2 \tag{4}$$

In the case of coupled resonance in liquids, the complex frequency shift ($\Delta f^*$) is given by eqn (6) (ref. 28 and 30) and introducing a parameter $\gamma$ with the dimension of frequency as

$$\gamma = \xi/m \tag{5}$$

$$\frac{\Delta f^*}{N_b} = \frac{\Delta f + i\Delta\Gamma}{N_b} = \frac{f_f}{N_b\pi Z_q}\frac{m\omega\left({\omega_b}^2 + i\omega_b\gamma\right)}{\omega^2 - {\omega_b}^2 - i\omega\gamma} \tag{6}$$

where $f_f$ is the fundamental frequency (5 MHz), $Z_q$ is the acoustic impedance of AT-cut quartz-crystal ($8.8 \times 10^6$ kg $m^{-2}$ $s^{-1}$), and $N_b$ is the number of adhering bacteria per unit area.

Eqn (6) represents a circular relation between bandwidth $\Delta\Gamma = \mathrm{Im}(\Delta f^*)$ *versus* frequency $\Delta f = \mathrm{Re}(\Delta f^*)$ shifts. The radii of such circles, $R_{pd}$, are proportional to the adhesive bond stiffness $k$ and can be calculated as[23]

$$2R_{pd} \approx \frac{\Delta\Gamma(\omega = \omega_b)}{N_b} \approx \frac{f_f}{N_b\pi Z_q}\frac{m\omega_b\left({\omega_b}^2 + i\omega_b\gamma\right)}{i\omega_b\gamma} \approx \frac{f_f}{N_b\pi Z_q}\frac{k}{\gamma} \tag{7}$$

assuming all bacterial cells possess the same bond stiffness and $\gamma \ll \omega_b$.[28]

### Atomic force microscopy and analysis

Glass slides were cleaned by sonication in 2% RBS35 (Omnilabo International BV, The Netherlands) for 3 min, followed by rinsing with tap water, demineralized water, methanol, tap water, and demineralized water again. A droplet of poly-L-lysine (0.01% α-poly-L-lysine with $M_w$ 70 000–150 000, Sigma-Aldrich, St Louis, Missouri, USA) was then spread over a cleaned glass slide and allowed to air dry to create a positively charged surface.[31] Next, the slide was rinsed with demineralized water and a droplet with suspended bacteria in 57 mM buffer was placed on the glass slide. After allowing the bacteria to adhere for 30 min, unbound bacteria were rinsed off with demineralized water and slides were put in 57 mM buffer for 1 h before initiation of AFM measurements, in order to mimic the conditions prevailing in the QCM-D experiments.

Bacteria were imaged over an area of 100 $\mu m^2$ at 0.5 Hz in the PeakForce-QNM mode on a BioScope Catalyst AFM (Bruker AXS, Santa Barbara, CA) using a PeakForce set-point of 2 nN. No bacteria were removed from the surface during the AFM scanning, indicating effective immobilization of the streptococci to the poly-L-lysine coating. The spring constant, $k$, and radius, $R$, of SCANASYST-FLUID AFM tips (Bruker AFM Probes, Camarillo, CA) were measured before each experiment using the resonance method at 150 kHz and scanning electron microscopy, respectively, and found to be around 1.2 N $m^{-1}$ and 18 nm, respectively.

AFM data were analyzed using Gwyddion1 2.26 (ref. 32) where a mask was created based on height data to identify the positions of immobilized bacteria and the force distant curves obtained at those locations were analyzed using the DMT channel of the AFM in order to obtain the Young's moduli. Assuming that the adhesion force between the tip and the bacterial cell surface can be neglected due to the use of a high frequency (1 kHz), this in essence yields a Hertzian contact model, which relates the force measured by the tip, $F_{tip}$, to the effective Young's modulus, $E$, according to

$$F_{tip} = \frac{4}{3}E\sqrt{Rd^2} \tag{8}$$

where $R$ is the radius of the AFM tip (18 nm) and $d$ is the deformation of the bacterial cell surface indicated by tip deflection. The effective Young's modulus $E$ is composed of two

 

components, due to the tip and the bacterial cell surface as given by eqn (9)

$$E = \frac{1}{\left[\frac{1-\nu_{tip}{}^2}{E_{tip}} + \frac{1-\nu_{bacterial\ surface}{}^2}{E_{bacterial\ surface}}\right]} \quad (9)$$

where $\nu$ is Poisson's ratio, taken as 0.5 for the bacterial cell surface. Since $E_{tip}$ is much larger than $E_{bacterial\ surface}$, eqn (9) simplifies to

$$E_{bacterial\ surface} = E(1 - \nu_{bacterial\ surface}{}^2) \quad (10)$$

The average Young's modulus of the bacterial cell surface, $E_{bacterial\ surface}$, over the locations identified by the height mask was obtained by applying a Gaussian fit through the data obtained for the different locations as identified by the height mask.

### TIRM and analysis

For TIRM, streptococci were allowed to adhere at room temperature for 5 min in 57 mM adhesion buffer to a glass cover slip in a disc-shaped parallel plate flow chamber, with a chamber height of 0.5 mm and an inner diameter of 12 mm. TIRM measurements were made under stagnant conditions in buffers with decreasing ionic strength. Buffers were replaced using a peristaltic pump at a flow rate of 150 μL $min^{-1}$. An inverted microscope (Olympus, IX71, Tokyo, Japan) in combination with a 100× apochromat TIRF-objective (NA 1.45, Olympus) and EMCCD camera (Andor iXon DU-885 Belfast, Northern Ireland) were used to observe the scattered light intensity from adhering bacteria in different ionic strength buffers. A laser (Coherent Innova 70, Santa Clara, CA, USA) with a wavelength of 488 nm was used for illumination, focused by a custom-made TIRM condenser onto the back-focal plane of the objective. The lateral distance of the focus from the back-focal plane could be varied using a nano-positioning stage in order to adjust the angle of incidence of the laser beam at the substratum surface. The laser power measured at the substratum surface was 200 μW at an angle of incidence of 0 degrees. During TIRM measurements, the angle of incidence was set at 63 degrees, resulting in an evanescent light field penetration depth $d_p$ of 183 nm according to

$$d_p = \frac{\lambda_0}{4\pi\sqrt{n_1{}^2\sin^2\theta - n_2{}^2}} \quad (11)$$

where $\lambda_0$ is the wavelength of the light in a vacuum, $\theta$ the incident angle at the glass–water interface and $n_1$ and $n_2$ the refractive indices of glass and the buffer, respectively. The buffer refractive index, $n_2$, was calculated based on the refractive index of water (1.333). A mirror, placed between the filter turret and the objective, in combination with a beam dump was used to prevent the reflected light from entering the EMCCD camera, therewith allowing detection of scattered light from the evanescent field only. The average scattering intensity from individual regions of interest drawn around six different adhering bacteria was measured on 100 frames for 5 ms. Changes in distance due to changes in ionic strength were calculated from the intensity of the scattered light according to[33]

$$I(z) = I_o e^{-z/d_p} \quad (12)$$

where $z$ denotes the distance from the interface, $I_o$ is the intensity at the interface ($z = 0$) and $d_p$ is the evanescent field penetration depth. The used buffers have slightly different refractive indices compared to water ($3.1 \times 10^{-5}$, $6.8 \times 10^{-5}$ and $31 \times 10^{-5}$ for buffers with ionic strengths 5.7, 12.5 and 57 mM, respectively (taken from the standard refractometry concentration table for NaCl)) causing a small deviation between calculated and real distance changes. This difference is estimated to be less than 2 nm with a distance change of 200 nm (with respect to water).

## Acknowledgements

We would like to thank ZON-MW for grant 91107008 enabling purchase of the quartz crystal microbalance Qsense-E1 & E4.

## References

1 L. Hall-Stoodley, J. W. Costerton and P. Stoodley, *Nat. Rev. Microbiol.*, 2004, **2**, 95–108.
2 B. J. Hall and L. Jones, *Eye Contact Lens*, 2010, **36**, 101–105.
3 S. H. Flint, H. van den Elzen, J. D. Brooks and P. J. Bremer, *Int. Dairy J.*, 1999, **9**, 429–436.
4 M. Hermansson, *Colloids Surf., B*, 1999, **14**, 105–119.
5 A. T. Poortinga, R. Bos, W. Norde and H. J. Busscher, *Surf. Sci. Rep.*, 2002, **47**, 3–32.
6 C. J. Rupp, C. A. Fux, A. Christoph and P. Stoodley, *Appl. Environ. Microbiol.*, 2005, **71**, 2175–2178.
7 H. J. Busscher, D. Jager, G. Finger, N. Schaefer and H. C. van der Mei, *Eur. J. Oral Sci.*, 2010, **118**, 177–182.
8 A. L. J. Olsson, H. C. van der Mei, H. J. Busscher and P. K. Sharma, *Langmuir*, 2010, **26**, 11113–11117.
9 R. Sonohara, N. Muramatsu, H. Ohshima and T. Kondo, *Biophys. Chem.*, 1995, **55**, 273–277.
10 N. I. Abu-Lail and T. A. Camesano, *Biomacromolecules*, 2003, **4**, 1000–1012.
11 J. D. Klein, A. R. Clapp and R. B. Dickinson, *J. Colloid Interface Sci.*, 2003, **261**, 379–385.
12 F. Rico, P. Roca-Cusachs, N. Gavara, R. Farre, M. Rotger and D. Navajas, *Phys. Rev. E: Stat., Nonlinear, Soft Matter Phys.*, 2005, **72**, 021914.
13 M. Berglin, E. Pinori, A. Sellborn, M. Andersson, M. Hulander and H. Elwing, *Langmuir*, 2009, **25**, 5602–5608.
14 L. Macakova, G. E. Yakubov, M. A. Plunkett and J. R. Stokes, *Colloids Surf., B*, 2010, **77**, 31–39.
15 G. Sauerbrey, *Z. Phys.*, 1959, **155**, 206–222.
16 J. Fatisson, R. F. Domingos, K. J. Wilkinson and N. Tufenkji, *Langmuir*, 2009, **25**, 6062–6069.
17 M. Berglin, A. Olsson and H. Elwing, *Macromol. Biosci.*, 2008, **8**, 410–416.
18 A. Olofsson, M. Hermansson and H. Elwing, *Appl. Environ. Microbiol.*, 2005, **71**, 2705–2712.
19 E. V. Olsen, S. T. Pathiriana, A. M. Samoylov, J. M. Barbaree, B. A. Chin, W. C. Neelt and V. Vodyanoy, *J. Microbiol. Methods*, 2003, **53**, 273–285.
20 A. L. J. Olsson, H. C. van der Mei, H. J. Busscher and P. K. Sharma, *Langmuir*, 2009, **25**, 1627–1632.
21 C. Poitras and N. Tufenkji, *Biosens. Bioelectron.*, 2009, **24**, 2137–2142.
22 X. Su and Y. Li, *Biosens. Bioelectron.*, 2005, **21**, 840–848.
23 R. D. Vaughan, C. K. O'Sullivan and G. G. Guilbault, *Enzyme Microb. Technol.*, 2001, **29**, 635–638.
24 A. L. J. Olsson, H. C. van der Mei, H. J. Busscher and P. K. Sharma, *J. Colloid Interface Sci.*, 2011, **357**, 135–138.
25 I. Marcus, M. Herzberg, S. Walker and V. Freger, *Langmuir*, 2012, **28**, 6396–6402.
26 A. H. Weerkamp, P. A. Handley, A. Baars and J. W. Slot, *J. Bacteriol.*, 1986, **165**, 746–755.
27 H. C. van der Mei, A. H. Weerkamp and H. J. Busscher, *FEMS Microbiol. Lett.*, 1987, **40**, 15–19.

28 A. L. J. Olsson, H. C. van der Mei, D. Johannsmann, H. J. Busscher and P. K. Sharma, *Anal. Chem.*, 2012, **84**, 4504–4512.
29 G. L. Dybwad, *J. Appl. Phys.*, 1985, **58**, 2789–2790.
30 A. Pomorska, D. Shchukin, R. Hammond, M. A. Cooper, G. Grundmeier and D. Johannsmann, *Anal. Chem.*, 2010, **82**, 2237–2242.
31 T. A. Camesano, M. J. Natan and B. E. Logan, *Langmuir*, 2000, **16**, 4563–4572.
32 D. Nečas and P. Klapetek, *Cent. Eur. J. Phys.*, 2012, **10**, 181–188.
33 J. Y. Walz, *Curr. Opin. Colloid Interface Sci.*, 1997, **2**, 600–606.



 